WRINKLE RIDGE FORMATION NORTH OF ORCUS PATERA, MARS

ANDREW GENDASZECK
Geology Department, Carleton College
Faculty Sponsor: Clint Cowan, Carleton College

MATHEW SILVER
Geology Department, Whitman College
Faculty Sponsor: Pat Spencer, Whitman College

INTRODUCTION

Wrinkle ridges are linear to sub-linear positive landforms produced by compression (Golombek et al., 1991; Schultz, 2000). They are common on several planetary bodies, including Mars, Earth, Venus, the Moon, and Mercury (see discussion in Schultz, 2000). On Mars they are typically found on ridged plains, which are inferred to consist of strong material such as basalt (Watters, 1991). The topography of these landforms is thought to reflect their internal structure and can thus provide insight into the mechanics of formation, which has previously been interpreted as the result of a combination of faulting and folding (Golombek et al, 1991). Important geometric parameters of wrinkle ridges include width, height and an elevation offset of topography on either side of the ridge (Figure 1) (Golombek et al., 2000). Elevation offsets are created by motion on dip-slip faults.

Several mechanical models to account for wrinkle ridges have been proposed; all include faulting but vary in the depth of penetration. One model proposes deep fault penetration (and thus requires the absence of a décollement) and does not require systematic spacing of ridges (Golombek et al., 1989; Golombek et al., 1991; Golombek et al., 2000). A contrasting model predicts that faulting takes place above a décollement and is the result of processes such as gravity creep (Watters, 1991) or some form of lithospheric compression (e.g., Suppe and Connors, 1992). Parallel, uniformly spaced ridges can be indicative of either scenario (Zuber and Aist, 1990), but if they occur on a regional slope, gravity creep is considered to be the more likely mechanism.

Currently orbiting Mars is the Mars Global Surveyor (MGS) spacecraft which contains, among other instruments, the Mars Orbiter Laser Altimeter (MOLA) (e.g. Smith et al., 1998). The MOLA provides much more accurate topographic data for Mars than any previously available from photoclinometry (e.g., Golombek et al., 1991) or Earth-based radar. MOLA data have a footprint spacing of ~330 m, a footprint size of ~130 m, and a vertical precision of ~30 cm (Zuber et al., 1992; Smith et al., 1999). In this study we use MOLA topographic data to characterize the morphology of north-south trending wrinkle ridges present in the lowlands north of Orcus Patera, and then compare these geometric data to the topography predicted for each type of fault model.

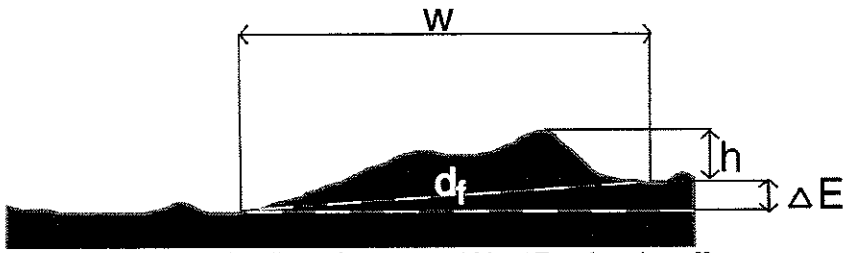

Figure 1: Wrinkle ridge dimensions: w = width, ΔE = elevation offset, h = height from crest to higher side, d_f = distance between the two endpoints of the ridge profile. V.E. ~50x.

METHODS

Because the ridges and the MOLA passes both trend approximately north-south, we used gridded data, 64 pixels per degree in longitude by 256 pixels per degree in latitude, to generate east-west topographic profiles perpendicular to the average trend of each ridge. *Gridview* (Roark et al., 2000), a

program that displays gridded topographic data, was used to calculate the east-west and north-south components of regional slope and to obtain topographic profiles across the ridges. Because wrinkle ridges are such subtle topographic features, we vertically exaggerated each profile to 50 times. For each profile, three geometric parameters (width, elevation offset, and height) were calculated using six data points: west-edge elevation, crest elevation, east-edge elevation, west-edge longitude, crest longitude, and east-edge longitude (Figure 1).

To discriminate between existing models, one cross-sectional wrinkle ridge profile was unfolded and measured in order to compare surface distance across the ridge after folding to the distance between the two endpoints of the ridge profile (Figure 1). For this same profile we calculated shortened horizontal distance due to faulting using elevation offset data and an assumed minimum fault dip of 25°.

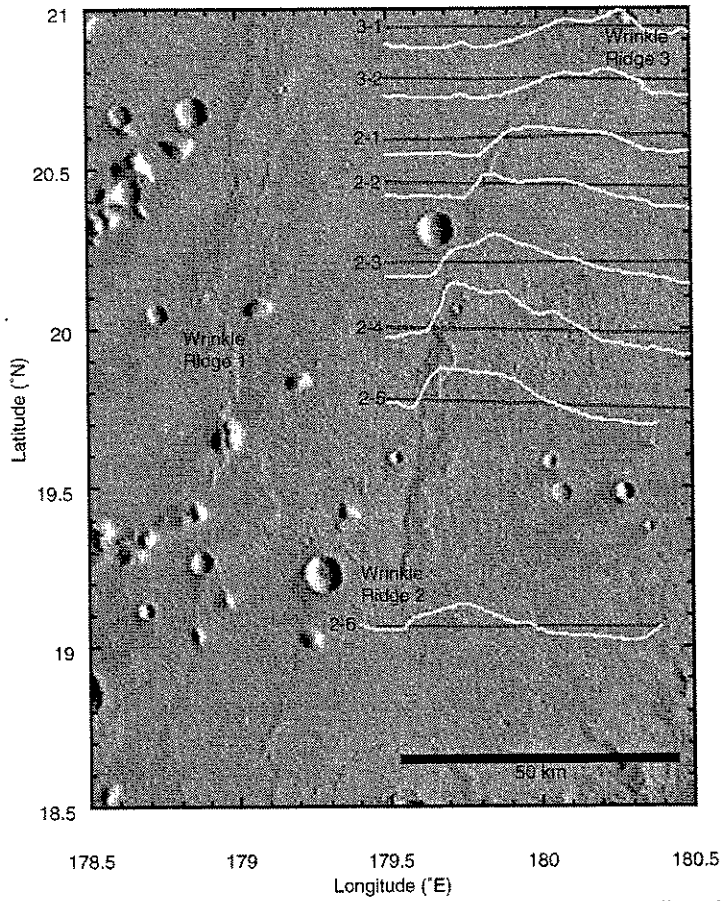

Figure 2: Three wrinkle ridges in the study area. Ridges are the N-S trending sinuous to linear features. Ridge profiles across two of the ridges are shown. E-W lines mark profile locations. Note uneven spacing, scale and wrinkle ridge dimensions. V.E. ~50.

RESULTS

We compiled fourteen *Gridview* topographic profiles, each approximately perpendicular to one of three ridges. Eight of the profiles are shown in Figure 2. For each profile we calculated the ridge's width, height, and elevation offset, as defined in Figure 1. Widths range from 33 to 54 km (±3 km) with an average of 41 km, heights range from 63 to 216 m (±1 m) with an average of 120 m, and elevation offsets range from 2 to 48 m (±1 m) with an average of 35 m; we find no evidence that the observed offsets are due to secondary processes (e.g., sediment deposition). Two other wrinkle ridges in our study area, located from 176.5°E to 178.5°E and from 19.5°N to 21°N, also show elevation offsets. On these two ridges, the higher side of the elevation offset is the east side for the western ridge and the west side for the eastern

ridge. Ridges in our study area are irregularly spaced and occur on a regional slope dipping 0.0002° eastward from 172°E to 188°E and 0.0006° southward from 22°N to 12°N. We measured an unfolded ridge width for a typical profile in our study and from it determined a shortening due to folding (S_{fold}) value (unfolded ridge width minus width as defined in Figure 1) of 9.5 m. Shortening due to faulting (S_{fault}), for the same ridge, is 76 m.

DISCUSSION

The topographic profiles we compiled show that wrinkle ridges in our study area are much broader than they appear in Viking images. The width of the ridges studied here is an average of 41 km with a standard deviation of 6 km. The profiles shown in Golombek et al., (1991) for wrinkle ridges in the Lunae Planum region, derived using photoclinometry, show average widths of 4.4 km with a standard deviation of 1.5 km. While we cannot directly compare the results of our study to those of Golombek et al., (1991) because different ridges were studied, lighting conditions in our study area would also lead us to infer such narrow widths in the absence of the MOLA data, and thus it seems likely that previous measurements made using photoclinometry may underestimate ridge width.

COMPARISON TO PROPOSED MODELS

The uniform spacing of wrinkle ridges has, in previous studies, been interpreted as the result of buckling of a plains unit at a critical wavelength (Zuber and Aist, 1990; Watters, 1991). Because the wrinkle ridges in our region are not spaced uniformly, it appears that they did not buckle at a critical wavelength. Instead, fault-propagation and/or fault-bend folding (Zuber and Aist, 1990) better explain the irregularity of ridge spacing.

Fault-bend and fault-propagation folding suggest a combination of faulting and folding to account for the observed wrinkle ridge morphology. The main difference between these two types of folds is that the fault breaks the surface in a fault-bend fold but does not in a fault-propagation fold. A comparison between S_{fault} and S_{fold} is typically used to determine which is the preferred model. Should S_{fault} greatly exceed S_{fold}, a fault-bend fold is inferred because the fault must break the surface to account for this comparison of strain. Otherwise, the fault tip dies in the subsurface and a fault-propagation fold is inferred (Golombek et al., 1991, Schultz, 2000). A typical profile in our study has a S_{fault}: S_{fold} value of 8 compared to 5-20 (Golombek et al., 1989) and 7 (Golombek et al., 1991). Our results, as well as those of (Golombek et al., 1989; Golombek et al., 1991), suggest that primary thrust faults beneath wrinkle ridges break the surface whereas smaller splay faults die in the fold and generate the "wrinkle". However, the occurrence of a simple fault-bend fold requires that width and height remain constant for a significant distance along strike and that elevation be conserved on either side of the fold (Golombek et al., 1991; Suppe and Connors, 1992; Schultz, 2000). From our data it is clear that elevation offsets are present and that the width and height of the ridges decrease toward each terminus. Thus, not even fault-bend folding can fully account for the surface morphology revealed in our data.

THIN-SKINNED VS. THICK-SKINNED DEFORMATION

A key issue addressed by many studies of wrinkle ridges is whether a regional décollement is present. If a décollement is present and deformation is due to gravity creep of material above it, a significant regional slope is required perpendicular to the ridges. Regional ridge-perpendicular slope for our study area, however, is only 0.0002°. In addition, if gravity creep were the deforming mechanism for these north-south trending wrinkle ridges, areas of high mass such as Elysium Mons to the west and the Tharsis region to the east are likely points of creep origin due to their high gravitational potential. This makes east-higher elevation offsets on ridges coming away from Tharsis and west-higher elevation offsets on ridges coming away from Elysium Mons most likely, with a transition somewhere in between. However, our profiles for the two laterally adjacent ridges discussed earlier show a geometry opposite to that expected from gravity creep: a plateau between the two ridges is higher than the level of the plains on the far sides of each ridge. If gravity creep is inferred this geometry can only be explained by backthrusting—not impossible but far less probable than forethrusting. Thus, the combination of the absence of a significant regional slope and the improbability of the above ridge geometry make thin-skinned deformation with gravity creep an unlikely mechanism.

The possibility exists that some thin-skinned process that is capable of acting without a regional slope produced these wrinkle ridges. However, our data do not support this possibility because the presence

of a décollement is incompatible with elevation offsets and varying width and height along strike (Golombek et al., 1989; Golombek et al., 1991; Schultz, 2000; Suppe and Connors, 1992). No known combination of folding and thrusting above a décollement can explain our basic geometric observations, so we contend that no décollement is present.

The depth of fault penetration, with the absence of a décollement, is simply calculated from the width of the ridge and an assumed minimum fault dip of 25° (Golombek et al., 1989; Golombek et al., 2000). This model predicts, based on average ridge widths, fault depth penetrations of 21 km and 17 km for the two wrinkle ridges we studied. A greater depth of penetration of 25 km is calculated by Golombek et al. (2000) for wrinkle ridges in Solis Planum but these authors assume that the faults extend from one ridge to the next; we assume only that the faults extend beneath the width of each ridge. In either case, the resulting depth of penetration compares to that of some known basement thrusts on Earth (e.g., Golombek et al., 1989).

CONCLUSIONS

Our data show that wrinkle ridges north of Orcus Patera are wide features with gentle topography. Due to the absence of a regional slope, we find gravity creep to be an unlikely mechanism for the formation of these ridges. Other possible mechanisms include fault-propagation and fault-bend folding: a strain comparison between faulting and folding shows that the thrust faults must break the surface, thus ruling out fault propagation folding, while the presence of elevation offsets as well as decreases in the width and height along strike lead us to believe that the ridges are not produced by fault-bend folding. We thus see deep-penetrating faults as the most plausible mechanism to account for observed wrinkle ridge morphology.

ACKNOWLEDGEMENTS

We would like to extend gratitude to the Keck Geology Consortium, the National Science Foundation, and the MOLA Science Team for funding, and to the Geodynamics Branch (Code 921) at NASA/Goddard Space Flight Center for hosting our research project. We additionally thank project faculty members Eric Grosfils (Pomoma College), Susan Sakimoto (GSFC), Carl Mendelson (Beloit College), and research assistant Jake Bleacher (now at Arizona State University). For data processing and visualization assistance we thank Martin Wong (UC Santa Barbara), Greg Neumann (MIT) and Jim Roark (SSAI).

REFERENCES

Golombek, M., Suppe, J., Narr, W., Plescia, J., and Banerdt, B., 1989, Involvement of the lithosphere in the formation of wrinkle ridges on Mars, *in* Watters, T. R., and Golombek, M. P., eds., MEVTV workshop on tectonic features on Mars: LPI Technical Report 89-06, p. 36-38.

Golombek, M. P., Anderson, F. S., and Zuber, M. T., 2000, Martian wrinkle ridge topography: Evidence for subsurface faults from MOLA [abstract]: Lunar and Planetary Science, no. XXXI, abstract 1294.

Golombek, M. P., Plescia, J. B., and Franklin, B. J., 1991, Faulting and folding in the formation of planetary wrinkle ridges: Proceedings of Lunar and Planetary Science, v. 21, p. 679-693.

Roark, J, Frey, H., and Sakimoto, S., 2000, Interactive graphics tools for analysis of MOLA and other data [abstract]: Lunar and Planetary Science, XXXI, abstract 2026.

Schultz, R. A., 2000, Localization of bedding plane slip and backthrust faults above blind thrust faults: Keys to wrinkle ridge structure: Journal of Geophysical Research, v. 105, no. E5, p. 12,035-12,052.

Smith, D. E., Zuber, M. T., Solomon, S. C., Phillips, R. J., Head, J. W., Garvin, J. G., Banerdt, B., Muhleman, D. O., Pettengill, G. H., Neumann, G. A., Lemoine, F. G., Abshire, J. B., Aharonson, O., Brown, C. D., Hauck, S. A., Inanov, A. B., McGOvern, P. J., Zwally, H. J., and Duxbury, T. C., 1999, The global topography of Mars and Implications for Surface Evolution: Science, v. 284, p. 1495-1503.

Suppe, J., and Connors, C., 1992, Critical taper wedge mechanics of fold-and- thrust belts on Venus: Initial results from Magellan: Journal of Geophysical Research, v. 97, no. E8, p. 13,545-13,561.
Watters, T. R., 1991, Origin of periodically spaced wrinkle ridges on the Tharsis plateau of Mars: Journal of Geophysical Research, v. 96, no. E1, p. 15,599-15,616.
Zuber, M. T., and Aist, L. L., 1990, The shallow structure of the Martian lithosphere in the vicinity of the ridged plains: Journal of Geophysical Research, v. 95, no. B9, p. 14,215-14,230.

MORPHOLOGY OF THE MARTE VALLES CHANNEL SYSTEM, MARS

KATHERINE E. POULTER
Department of Geology, The Colorado College, Colorado Springs, CO 80903
Sponsor: Eric Leonard, The Colorado College

SVEN C. MOLLER
Department of Geology, Pomona College, Claremont, CA 91711
Sponsor: Eric Grosfils, Pomona College

INTRODUCTION

We are interested in the origins and evolution of the fluvial channels of Marte Valles, located along the southeastern edge of Orcus Patera in the Elysium region of Mars (Fig. 1). Although ancient highland fluvial networks and the dramatic outflow channels such as Kasei Valles on the dichotomy boundary have been intensively studied (e.g., Baker, 1982; Komatsu and Baker, 1997), relatively little effort has been devoted to studying some of the low-relief drainage systems in the northern lowlands. The high-resolution topography data from the Mars Orbiter Laser Altimeter (MOLA) (Zuber et al., 1992; Smith et al., 1998), flown on the Mars Global Surveyor (MGS) spacecraft, allow careful study of lowland channels that were difficult or impossible to distinguish with topography mapped by the USGS using Viking images.

The Marte Valles channel system looks similar in shape if not in scale to the Martian outflow channels of Kasei Valles, which are hypothesized to be the result of volcanically induced catastrophic flooding. Baker and Milton (1974) propose the Channeled Scabland of Washington, site of the glacial Lake Missoula outburst floods, as a terrestrial analogue for the Martian outflow channels. A more recent study of Kasei Valles with MOLA data, however, suggests evidence of repeated flooding over a longer period of time (Williams et al., 2000). Subsequent research has suggested several possible source mechanisms for Martian outflow channels: episodic aquifer release (Carr, 1979), a pluton-driven hydrothermal system (Gulick, 1998), or volcanic-

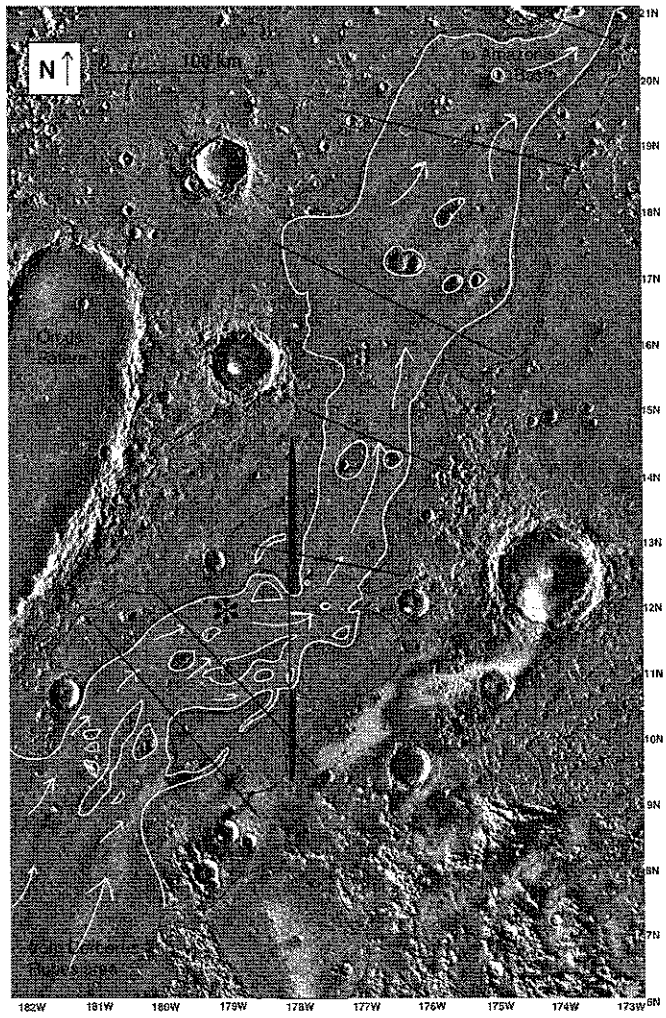

Figure 1: A mosaic of Viking images with superimposed white Marte Valles channel boundaries and white arrows indicating flow directions. Areas circled in thin black show resurfacing adjacent to the channel; filled black ellipses indicate wrinkle ridge remnants. Profiles were taken where thick black lines cross the channel and an ✻ marks the Mars Orbital Camera image location (Figure 2).